Routes to the preparation of mixed monolayers of fluorinated and hydrogenated alkanetiolates grafted on the surface of gold nanoparticles

Maria Şologan,[a] Cristina Cantarutti,[a] Silvia Bidoggia,[a] Stefano Polizzi,[b] Paolo Pengo,[a] and Lucia Pasquato*,[a]

[a] *Department of Chemical and Pharmaceutical Sciences and INSTM Trieste Unit, University of Trieste, via L. Giorgieri 1, 34127 Trieste, Italy. E-mail: lpasquato@units.it*

[b] *Department of Molecular Sciences and Nanosystems, University Ca' Foscari of Venezia, Via Torino 155/b, I-30172 Venezia-Mestre, Italy*

Abstract

The use of binary blends of hydrogenated and fluorinated alkanethiolates represents an interesting approach to the construction of anisotropic hybrid organic-inorganic nanoparticles since the fluorinated and hydrogenated components are expected to self-sort on the nanoparticles surface because of their reciprocal phobicity. These mixed monolayers are therefore strongly non-ideal binary systems. The synthetic routes we explored to achieve mixed monolayer gold nanoparticles displaying hydrogenated and fluorinated ligands clearly show that the final monolayer composition is a non-linear function of the initial reaction mixture. Our data suggest that, under certain geometrical constraints, nucleation and growth of fluorinated domains could be the initial event in the formation of these mixed monolayers. The onset of domains formation depends on the structure of the fluorinated and hydrogenated species. The solubility of the mixed monolayer nanoparticles displayed a marked discontinuity as a function of the monolayer composition. When the content of the fluorinated component is small, the nanoparticle systems are fully soluble in chloroform, at intermediate content the nanoparticles become soluble in hexane and eventually they become soluble in fluorinated solvents only. The intervals of monolayer compositions in which the solubility transitions are observed depend on the nature of the thiols composing the monolayer.

1 Introduction

In the recent years, a significant interest on the development of gold nanoparticles protected by monolayers comprising fluorinated ligands started to emerge[1] and the now available strategies to improve their solubility,[2,3] in addition to remarkable examples of their properties,[4-7] will likely stimulate future developments. Our previous studies, carried out on mixed monolayer gold nanoparticles (MMNPs) protected by blends of fluorinated (*F*-) and hydrogenated (*H*-) amphiphilic thiolates, demonstrated that phase segregation triggered by, *inter alia*, the reciprocal phobicity of the dislike thiolates is operative and can be observed even using less than 5% of *F*-ligands.[8,9] Self-sorting of hydrogenated and fluorinated compounds is known to occur in the bulk phases,[10,11] in supramolecular assemblies both at the micro-[12,13] and nano-scale,[14-19] regime or even at the molecular level.[20,21] We believe that fluorophilic/fluorophobic interactions will also represent a powerful tool in the controlled formation of domains of well-defined morphology in the monolayer of gold nanoparticles. The morphological features of mixed monolayers are central in determining the properties of nanoparticles such as their solubility behaviour and wettability;[22] their interaction with biological membranes;[23-25] their assembling properties[26] and catalytic activity.[27] A large body of experimental evidences[28-35] and theoretical investigations[36-40] provided a valuable framework of understanding of the factors governing the formation of domains in the monolayer of gold nanoparticles and other nanosized structures.[41] However, despite these outstanding achievements, there is a lack of comprehensive experimental data concerning the preparation of MMNPs. Even for well characterised MMNPs, the information on how differences in molecular structures of the ligands used in the synthesis impact on the final composition of the monolayer are only sparse. It is often assumed that the stoichiometric ratio of the ligands used in the synthesis is equal to the ratio on the ligand shell,[29] and in some cases evidences do exist.[35] In other cases, only the composition of MMNPs is reported but not the ratio of the thiols used in the synthesis.[42] In a different route to MMNPs that exploits the assembly of mixtures of thiols on the surface of dioctylamine-capped gold nanoparticles,[43,44] it was also reported that the final composition of the monolayer reflects the initial composition of the ligand mixture. On the contrary, the place exchange reaction is known to be sensitive to the structure of the incoming thiols, with the equilibrium position depending on their length and steric bulk.[45]

Exploiting the fluorophobic-fluorophilic interactions between *F*- and *H*-thiolates may represent an advantageous additional tool to control the morphology of mixed monolayers. This approach, if successful, will allow bringing the "chemical mismatch" between ligands to a maximum; hence maximizing the phase segregation behaviour. However, the preparation of *F*-/*H*-MMNPs is, at present, only little explored. No comprehensive data on the synthetic conditions needed to introduce

a given amount of fluorinated components in the monolayer of nanoparticles and their dependence on the thiols molecular structure are presently available. Moreover, the different bulkiness of *F*- versus *H*-alkyl chains adds complexity to such an investigation. Based on these considerations we realised the urgency of a fundamental analysis addressing this gap.

Understanding how the final monolayer composition depends on the initial composition of the reaction mixture in either the direct synthesis or in the place exchange reaction is thus instrumental to any approaches based on the use of *F*- and *H*-thiols for the preparation of MMNPs. We reasoned that the only way to investigate the point in details was to reduce the complexity of the systems to a minimum using simple fluorinated and hydrogenated model thiols of different length and steric bulk and exploring a wide range of monolayer compositions. Based on the experimental data, we discuss the correlation between the initial ratio of the thiols and the final composition of the monolayer in relation to the structure of the ligands. We also correlate the core size of the MMNPs to the nature of the thiols. Finally, we analyse the effect of the monolayer composition on the solubility properties of MMNPs.

2 Results and discussion

2.1 Design of the approach for the preparation of MMNPs. Aiming at exploring a broad range of conditions for the preparation of gold nanoparticles displaying mixed monolayers of *H*- and *F*-ligands and analysing how the monolayer composition depends on the ligands structure, we devised the library of simple thiols displayed in Figure 1A. The fluorinated thiols we used are 1*H*,1*H*,2*H*,2*H*-perfluorooctanethiol (**HF6**)[†] and 1*H*,1*H*,2*H*,2*H*-perfluorododecanethiol (**HF10**) while the hydrogenated thiols are dodecanethiol (**HC12**), octanethiol (**HC8**), hexadecanethiol (**HC16**) and 3-methyldodecane-1-thiol (**HbrC12**). The thiols **HF6**, **HC8**, **HC16** and **HC12** are commercially available; thiol **HbrC12** was synthesised according to Scheme S1 of the Electronic Supplementary Information (ESI) while thiol **HF10** was prepared according to literature procedures.[46] The structural diversity of the thiols reported in Figure 1A was conceived in order to analyse how structural parameters such as the thiols length, length mismatch and steric bulk, influence the outcome of the syntheses.

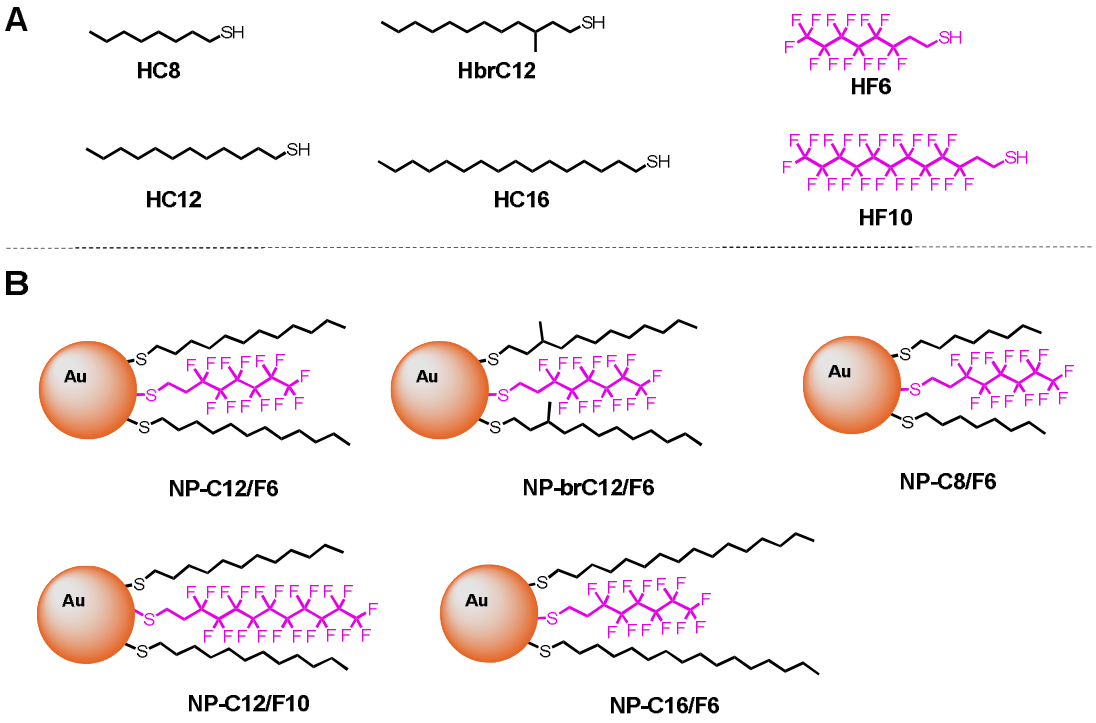

Figure 1. Panel A: library of the hydrogenated and fluorinated thiols used in this study. Panel B: structures of the mixed monolayer nanoparticles prepared by combining the thiols reported in panel A.

The combination of thiols **HC12** and **HF10** in nanoparticles **NP-C12/F10**[‡] or thiols **HC8** and **HF6** in nanoparticles **NP-C8/F6** will allow an analysis of the conditions required for the preparation of MMNPs displaying *H*- and *F*-ligands of the same length. The combination of thiols **HC12** and **HF6** in nanoparticles **NP-C12/F6** or thiols **HC16** and **HF6** in nanoparticles **NP-C16/F6**, allows instead an analysis of the role played by the length mismatch (4 atoms and 8 atoms respectively) in the outcome of the syntheses. By combining thiols **HbrC12** and **HF6** in nanoparticles **NP-brC12/F6** we will explore the effect of using a branched thiol preventing the formation of a monolayer stabilised by van der Waals interactions,[42] in association with a four atom shorter fluorinated thiol. A cartoon representation of the MMNPs discussed is presented in Figure 1B.

2.2 Nanoparticles synthesis. The preparation of the MMNPs **NP-C16/F6**, **NP-C8/F6**, and **NP-brC12/F6** was achieved by direct synthesis following the Brust-Schiffrin procedure employing a blend of the *H*- and *F*-thiols. Otherwise, **NP-C12/F6** and **NP-C12/F10** were prepared by place exchange on nanoparticles bearing monolayers comprising hydrogenated thiolates only. For the preparation of the MMNPs by place exchange, narrowly dispersed **NP-C12** were prepared by the method of Miyake.[47] The use of two different methodologies for the preparation of MMNPs is particularly relevant because mass analyses give evidence that mixed monolayers obtained by direct synthesis display little phase segregation, while ligand self-sorting seems to be more pronounced for

the systems obtained by place exchange.[48] The ratio between *H*- and *F*-thiolates in the monolayer was assessed by decomposing a small amount of nanoparticles in the presence of excess iodine. The mixture of disulfides thus obtained was analysed by ^{1}H NMR and the ratio between the two thiolates present in the monolayer was determined by integration of the signals due to the methylene group in the alpha position to the sulfur atom.

The diameters of the nanoparticles core were determined by TEM and the amount of organic material was assessed by thermogravimetric analyses. In some cases in both the direct synthesis and the place exchange reactions, two or three minor fractions of nanoparticles (all fractions from the same synthesis are indicated in the tables with the same lowercase letter) could be separated by exploiting their different solubility in chloroform, hexane and/or hexafluorobenzene. All of these fractions have been completely characterised. The solubility properties of these nanoparticles are indicated by adding (C); (H) or (F) to their designation, to indicate solubility in chloroform, hexane or hexafluorobenzene respectively as reported in Table S1, Table S2, Table S6 and Table S8 of ESI for some examples.

2.3 Analysis of the monolayer composition and composition-related properties. Prior to presenting our analysis of the composition of mixed monolayers as a function of the relative amount of thiols in the initial reaction mixture, we find it useful defining the limiting behaviours expected under place exchange conditions or in the direct synthesis. Let us consider the following cases: (i) the preparation of MMNPs by place exchange of thiol B from homoligand nanoparticles comprising thiolates A only. (ii) The preparation of MMNPs obtained by direct synthesis using a blend of thiols A and B. For the sake of simplicity, we shall consider the formation of a single population of nanoparticles.

Mixed monolayer obtained by place exchange. The relationship between the molar fraction of ligand B in the monolayer and its initial molar fraction in the reaction mixture can conveniently be represented in the plot of Figure 2. In this plot, the x-axis represents the initial molar fraction of thiol B in the reaction mixture, while the y-axis represents the final composition of the monolayer expressed as molar fraction of the thiolate B.

Three different limiting cases are theoretically possible depending on the relative affinity of thiols A and B and the thermodynamics of the monolayer formation. If we assume that the ligands B have a very high tendency to assemble in the monolayer and that this is much higher than that of thiols A, in the place exchange reaction ligands B will displace the ligands A completely. The amount of ligand B introduced in the monolayer is only limited by its initial molar fraction. This process will lead, eventually, to the complete conversion of the homoligand A-monolayer into a homoligand B-

monolayer when the initial molar fraction of B is just 0.5, red curve in Figure 2; any further increase of the initial molar fraction of thiol B cannot produce further changes. A second limiting behaviour is obtained when no preference between ligand A and ligand B in forming the monolayer exists. The final compositions of the monolayers as a function of the initial compositions will thus cluster along the diagonal of the plot, blue line in Figure 2. A third limiting case is the one pertaining to a situation in which the grafting of ligand B is strongly disfavoured, green line in Figure 2. In this case, no B ligands will be found in the monolayer at any initial molar fraction.

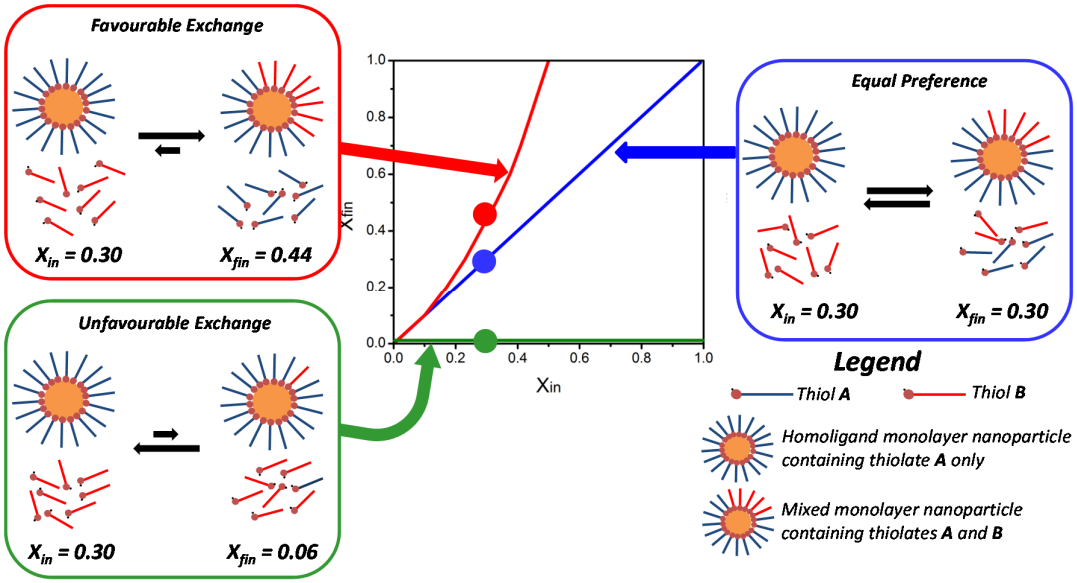

Figure 2. Limiting cases theoretically possible in the place exchange between thiols B and homoligand nanoparticles featuring the thiolate A only. If the grafting of thiols B is favoured, top left of the figure; complete consumption of thiols B can take place with displacement of an equal amount of thiolate A. In this case, the experimental data points will cluster along the red curve. If the grafting of thiol B is disfavoured, bottom left of the figure, only little exchange will be observed and the experimental data will be found close to the green line of the plot. If there is equal preference for the grafting of ligands A or B, right hand side of the figure, the composition of the mixed monolayer will reflect the initial composition of the reaction mixture and the experimental data points will cluster along the diagonal of the plot.

Mixed monolayer obtained by direct synthesis. In the direct synthesis of MMNPs, the thiols are in excess with respect to the available grafting sites on the nanoparticle surface.[§] This is a remarkable difference with respect to place exchange. If ligands B have a very high affinity for the monolayer and this is much higher than the affinity of the thiols A, it is theoretically possible to end-up with homoligand B-monolayers even if the initial molar fraction of thiol B is relatively small. In this case the experimental data point could be found either above the red line of Figure 2 or close to it. On the other hand, if there is no preference for the grafting of the A or B thiolates, the experimental data point will cluster along the diagonal of the plot. If the grafting of thiols B is disfavoured the experimental points will be found beneath the diagonal or approaching the green line of the plot of Figure 2.

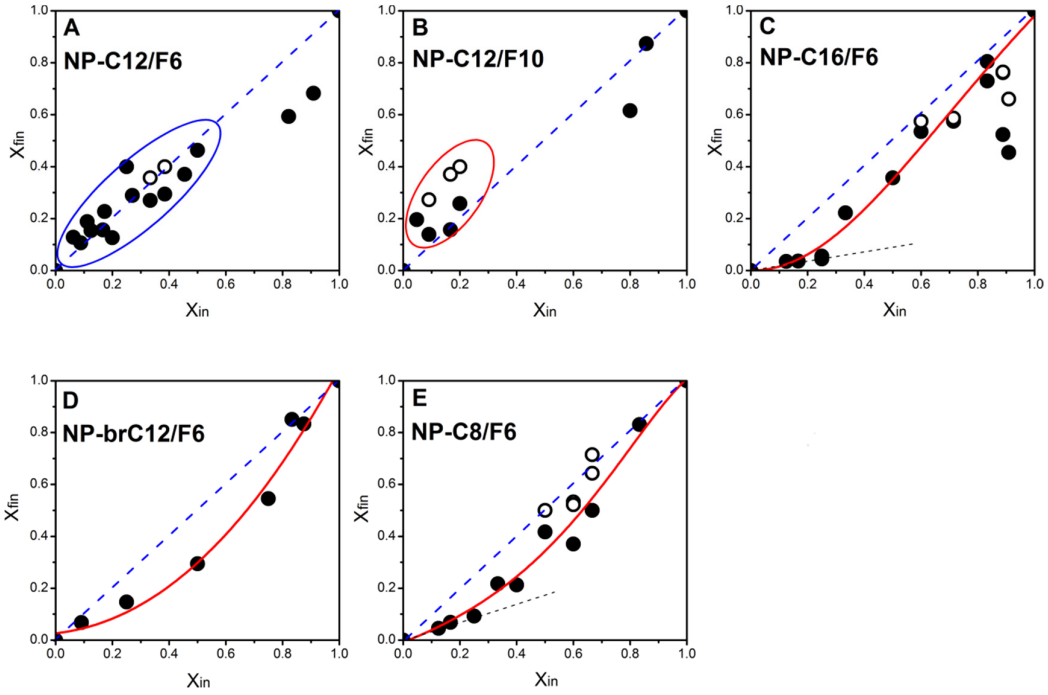

Figure 3. Panel A and B: experimental data of the monolayer compositions for nanoparticles **NP-C12/F6** and **NP-C12/F10**, respectively, as a function of the composition of the initial reaction mixture. Panel C, D, and E: experimental data of the monolayer compositions for nanoparticles **NP-C16/F6**, **NP-brC12/F6**, and **NP-C8/F6**, respectively, as a function of the composition of the initial reaction mixture.

Analysis of the experimental data for the synthesis of the mixed monolayer nanoparticles. For nanoparticles **NP-C12/F6**, Figure 3A, the experimental data cluster along the diagonal of the plot, with some deviations only at very high initial loading of the fluorinated component. Hence, from a synthetic point of view, the preparation of nanoparticles **NP-C12/F6** containing up to 50% of the fluorinated ligand is straightforward, since the initial molar fraction of the reaction mixture is maintained in the final product. This indicates that there is essentially no energetic penalty or gain in introducing thiol **HF6** in the monolayer of preformed **NP-C12**. Instead, some energetic penalty, resulting in a less facile introduction of the *F*-ligand in the monolayer, occurs only when the initial molar fraction is very high. In some cases, the synthesis of nanoparticles **NP-C12/F6** gives rise to a sub-population of nanoparticles with different solubility properties and richer in the fluorinated component that could be isolated, nanoparticles **NP-C12/F6-i(H)** and **NP-C12/F6-k(H)**, Table S1. The compositions of these systems are reported as open symbols in the plot of Figure 3A.

Similarly, for nanoparticles **NP-C12/F10**, Figure 3B, the experimental data points tend to cluster close or slightly above the diagonal. As in the previous case, in the preparation of nanoparticles **NP-C12/F10**, a small fraction of nanoparticles with monolayer very rich in the fluorinated component could be isolated, nanoparticles **NP-C12/F10-a(H)**, **NP-C12/F10-b(H)** and **NP-C12/F10-d(H)**, Table S2. The composition of these nanoparticles is reported with open symbols in the plot of

Figure 3B. These data indicate a facile introduction of the fluorinated ligands in the monolayer of the nanoparticles even at low molar fraction of the fluorinated component in the reaction mixture.

Increasing the length difference between the ligands as in nanoparticles **NP-C16/F6** a completely different behaviour was observed, Figure 3C; in facts, the introduction of few *F*-ligands in the monolayer of these nanoparticles proved to be extremely unfavourable with a strong negative deviation from the diagonal of the plot in the region of small initial fraction of the *F*-component. In these syntheses more than 20% of fluorinated ligand in the reaction mixture was necessary to achieve a mixed monolayer containing a mere 5% of fluorinated thiolates. After this threshold, however, the introduction of fluorinated ligands becomes more facile, with the experimental data points approaching the diagonal of the plot. Also in this case we observed the formation of sub-populations of nanoparticles richer in the fluorinated component, but, at variance with **NP-C12/F6** and **NP-C12/F10**, this was observed only at initial molar fractions of the *F*-component higher than 60%; the compositions of these systems are reported with open symbols in the plot of Figure 3C.

For nanoparticles **NP-brC12/F6**, Figure 3D, yet a different behaviour appears. In this case the introduction of *F*-ligands remains unfavourable in all of the conditions explored. This is not unexpected because, by design and in analogy with literature evidences, these nanoparticles are believed to display a poorly organised monolayer. Notably for nanoparticles **NP-brC12/F6**, we could not identify sub-populations of nanoparticles with different contents of the fluorinated ligands obtained in the same synthesis.

A somewhat intermediate behaviour was observed for nanoparticles **NP-C8/F6**, Figure 3E, for which more than 20% of *F*-ligand in the reaction mixture was needed to achieve a 10% of the *F*-thiolate in the final monolayer composition. After this threshold the introduction of *F*-ligands becomes more favourable, with the experimental data points slowly approaching the diagonal of the plot at higher molar fraction of **HF6**. In some cases, the preparation of nanoparticles **NP-C8/F6** yielded a small fraction richer in the fluorinated component when the initial composition of the reaction mixture contained more than 50% of the *F*-ligand. The compositions of these systems are reported with open symbols in the plot of Figure 3E.

From these data it is clear that the formation of mixed monolayers comprising fluorinated thiolates may be favoured or disfavoured depending on the structure of the ligands and the degree of substitution that is achieved; relatively subtle structural changes impact considerably on the outcome of the syntheses. Most importantly, these data display that the final composition of the MMNPs cannot be *a priori* predicted on the basis of the composition of the reaction mixture, neither in the direct synthesis, nor in the place exchange reaction.

Effect of the fluorinated ligand loading on the nanoparticles size. It is well established by a large number of experimental evidences that in the Brust-Schiffrin synthesis, the size of gold nanoparticles can be tuned by varying the initial gold/thiol ratio; the larger the ratio, the larger the resulting nanoparticles.[49] There are also evidences that bulky thiols tend to favour the formation of smaller gold nanoparticles.[50] Fluorocarbons have a cross-sectional area of 28.3 $Å^2$ while for hydrocarbons the molecular cross section is 18.9 $Å^2$ only.[51] The fluorinated thiols used in this study are therefore much bulkier (1.5 times higher cross-sectional area) than the hydrogenated ligands, with the possible exception of the branched **HbrC12**. It is expected that the introduction of *F*-ligands in the monolayer of gold nanoparticles may result in systems of small size. In the Brust-Schiffrin synthesis of MMNPs we indeed observed a monotonous decrease of the nanoparticles size increasing the molar fraction of the *F*-component in the initial reaction mixture while maintaining constant the total gold/thiols ratio. This behaviour was found to be general; regardless the difference in length between the *F*- and *H*-ligands and the steric bulk of the hydrogenated thiols. The experimental data for the nanoparticles **NP-C8/F6**, **NP-C16/F6** and **NP-brC12/F6** are reported in Figures 4A, 4B, and 4C respectively. The size contraction observed when a large molar fraction of the *F*-ligands is used has clearly a significant impact in the choice of the reaction conditions. In addition, it is also likely to have an impact on the organization of the monolayer since the morphology of mixed monolayers depends also on the nanoparticle curvature radius and in turn on the free volume available per chain.

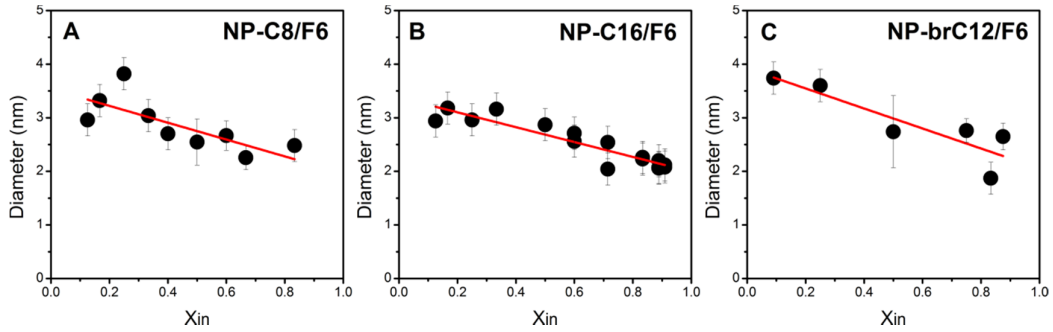

Figure 4. Dependence of the nanoparticles core diameter on the initial molar fraction of the fluorinated ligand. Error bars represent the standard deviation of the average diameter measured from TEM analyses. In the case of multiple preparations with the same initial loading of the fluorinated component, the experimental points represent the average of the diameters and error bars represent their standard deviation.

Solubility behaviour of MMNP. The solubility properties of these nanoparticles systems are very informative and were found to vary according to the amount of fluorinated ligand in the monolayer and the structure of the fluorinated and hydrogenated thiolates. At low molar fraction of the fluorinated component, the nanoparticles were freely soluble in chloroform and methylene chloride. At intermediate content of the fluorinated component, the nanoparticles were soluble in hexane,

while at the higher molar fractions, they were soluble in fluorinated solvents only. In all of the cases, the solubility limit in the different solvents was higher than about 10 mg/mL. To qualitatively analyse the solubility behaviour in relation to the monolayer composition, we found it convenient to use the solubility in the different solvents as a categorical variable and to plot this variable against the monolayer composition expressed as molar fraction of the *F*-ligand, Figure 5.

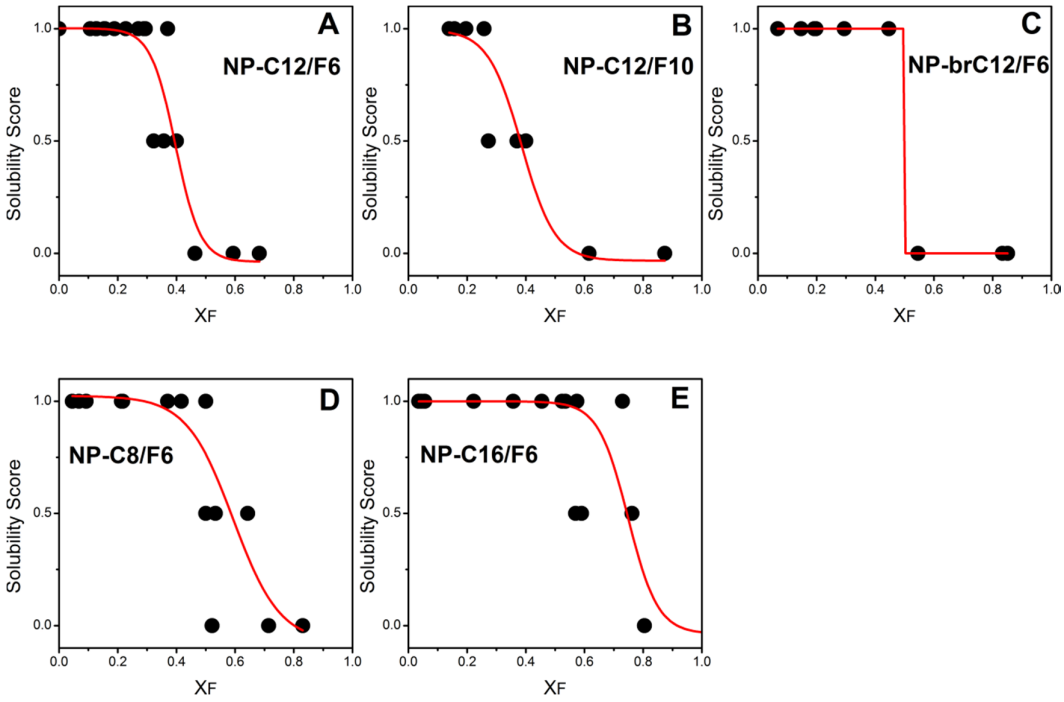

Figure 5. Comparison of the solubility transitions for the MMNPs as a function of the molar fraction of fluorinated component in the monolayer. The solubility is expressed according to the following score: score = 1 is assigned to the nanoparticles soluble in chloroform. Score = 0.5 is assigned to the nanoparticles soluble in hexane, score = 0 is assigned to the nanoparticles soluble in hexafluorobenzene.

To the systems fully soluble in chloroform we arbitrarily assigned a score of 1, the nanoparticles systems soluble in hexane were ranked with a score of 0.5 and those soluble in fluorinated solvents only (hexafluorobenzene was used throughout the study) were ranked with a score of zero. This approach allows to simply comparing the solubility properties of different set of nanoparticles. Nanoparticles **NP-C12/F6** display a solubility transition, corresponding to the onset of solubility in hexane, when about 40% of the fluorinated thiolate is present in the monolayer; the same percentage was found for nanoparticles **NP-C12/F10**. A significant difference was instead observed for nanoparticles **NP-C16/F6** that remained fully soluble up to a molar fraction of fluorinated ligand of 0.8. For nanoparticles **NP-brC12/F6**, the transition occurred when the molar fraction of the *F*-ligand was 0.5, the same behaviour was found for nanoparticles **NP-C8/F6**.

2.4 Discussion

A rationalization of the experimental evidences presented above can be put forth by considering that the immiscibility of *H*- and *F*-ligands may lead to self-sorting of the two species and that their difference in length and/or steric bulk may substantially contribute to the driving force of the self-sorting process.

Direct evidences of these phenomena have been already reported for mixtures of *H*- and *F*-ligands;[9] further detailed studies addressing the influence of the ligand structure in determining the extent of clustering and the monolayer morphologies of the MMNPs presented here are ongoing in our lab. From a general point of view, if short fluorinated thiolates tend to cluster in a monolayer of longer hydrogenated ligands, the introduction of a very small number of *F*-ligands in the monolayer will be unfavourable. This is because introducing a few fluorinated ligands will decrease the number of van der Waals contacts between hydrogenated chains without offering a significant enthalpic gain deriving from the establishment of fluorophilic interactions. In addition an unfavourable *H*/*F* interface will be formed. At this stage the entropic gain due to the increased conformational mobility of the hydrogenated thiolates will also be minimal. Only when the amount of the *F*-ligands exceeds a certain threshold, the introduction of more fluorinated ligands should become favourable because of the increased number of fluorophilic interactions and the increased entropic gain associated to the conformational mobility of the longer hydrogenated thiolates. This is reminiscent of a cooperative process, where the (unfavourable) introduction of the first few fluorinated ligands generates the conditions for a more favourable assembling. We can clearly trace this phenomenon to the synthetic conditions explored for the preparation of nanoparticles **NP-C16/F6**, Figure 3C. In this case the introduction of up to 5% of fluorinated ligands is strongly disfavoured, while after this threshold it becomes more favourable. The change in slope in the plot of Figure 3C is consistent with the cooperative mechanism outlined above; in the first phase a few nucleation centres are formed that eventually evolve towards the growth of fluorinated domains. Nucleation and growth of alkanethiolate monolayers by displacement of weakly bound ligands on the surface of gold nanoparticles have indeed ben reported.[52] Our data may be taken as an indication that in the case of nanoparticles **NP-C16/F6**, 5% of the *F*-ligand is sufficient to trigger the formation of fluorinated domains. This percentage is very close to the results of our previous studies displaying that already at the 5% loading, domains are formed in mixed monolayers comprising amphiphilic *H*- and *F*-ligands.[9] Another remarkable property of **NP-C16/F6** is that up to 80% of the fluorinated ligand can be introduced without significantly affecting the solubility of the system. This implies that the *F*-ligands cannot form large solvent exposed domains that would trigger the particles aggregation. On the other hand, the data of Figure 3C do suggest that domains indeed exist implying that these

should be relatively small and/or shielded from the solvent and from the fluorinated domains of other nanoparticles by the longer *H*-ligands.

For nanoparticles **NP-C12/F10**, the experimental data points cluster slightly above the diagonal of the plot of Figure 3B indicating that the introduction of the *F*-ligands in the monolayer is favourable even at low loading of the fluorinated component. It should also be noted that for these nanoparticles we observed the formation of a second population of nanoparticles with high content of the fluorinated ligand and different solubility properties even when only 10% of thiol **HF10** was used in the place exchange reaction. Taken together, these data, suggest a strong tendency of **F10** to be assembled in the monolayer of nanoparticles **NP-C12/F10**. When, as in this case, there is no length mismatch between the thiolates, the enthalpic balance due to the loss of interactions between hydrogenated ligands and the establishment of fluorophilic interactions will be a significant contribution to the overall ΔG of reaction; a further (unfavourable) contribution to the ΔG of reaction will be the formation of an *H*/*F* interface. Based on our experimental evidences, it is reasonable to think that for **NP-C12/F10**, clustering of ligands is likely to occur initially with the formation of small patches, eventually evolving towards larger compact domains, minimising in all cases the unfavourable formation of *H*/*F* interfaces.

The TEM image of **NP-C12/F10-b** drop casted from a 10 ng/mL chloroform solution, Figure 6, displays the formation of nanoparticle dimers and trimers accounting for the 50% of the total population. As comparison, the TEM image of **NP-C12/F6 –k(H)**, in the same conditions, shows a 15% of dimers and trimers over the total nanoparticles population. This specific self-assembly pattern supports the existence of a well-defined anisotropy in the nanoparticles monolayer, consistent with the presence of large fluorinated and hydrogenated domains. The aggregation is likely due to the interaction of the fluorinated domains pertaining to different particles.

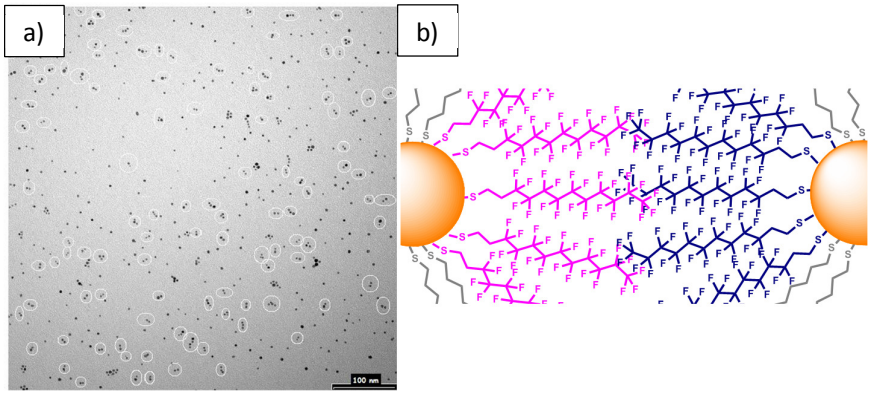

Figure 6. a) TEM image (magnification of 140K x) of nanoparticles **NP-C12/F10-b** drop casted from a 10 ng/mL chloroform solution. Dimers, trimers and some higher oligomers are encircled in white. b) Schematic representation of interdigitation between fluorinated ligands pertaining to different Janus nanoparticles.

Given the absence of length mismatch between the two thiols **HC12** and **HF10**, the observed behaviour is consistent with Glotzer's theoretical prediction of Janus nanoparticles.

As in the preceding case, the experimental data for nanoparticles **NP-C12/F6**, Figure 3A, indicate that there is essentially no energetic penalty or gain in introducing thiol **HF6** in the monolayer of preformed **NP-C12** up to a final composition of 50%. Since, experimentally, the introduction of the fluorinated ligand was found to be easy even at very low loading, we expect the initial formation of small domains as in the case of **NP-C12/F10**. However, at variance with the previous case, for nanoparticles **NP-C12/F6** a docecanethiolate unit is replaced by the four atom shorter **F6** unit. If clustering of the fluorinated ligands takes place, this geometrical mismatch should produce an increased conformational freedom for the hydrogenated ligands at the boundaries of the *F*- ligands clusters. In this case domains with a large interfacial area to surface ratio could be expected.

The solubility properties of both nanoparticles **NP-C12/F6** and **NP-C12/F10**, are in keeping with the formation of clusters of ligands, leading to the onset of low solubility already when about only 40% of the *F*- ligands are introduced in the monolayer, Figure 5A and Figure 5B respectively.

For nanoparticles **NP-brC12/F6**, the experimental data points cluster beneath the diagonal of the plot of Figure 3D, suggesting an unfavourable assembling of the ligand **F6** in the nanoparticles monolayer. Since in this case the branched nature of the **brC12** thiolate hinders the formation of a compact monolayer, the formation of domains will be unlikely and a random distribution of the thiolates on the monolayer will result, in analogy to the observation of Stellacci and co-workers.[42] The absence of fluorinated domains is consistent with the solubility properties of these systems that remain soluble in chloroform up to the introduction of 50% of the fluorinated component. Experimental evidence that is consistent with a random distribution of the thiolates is also the absence of sub-populations of nanoparticles, obtained in the same synthesis but displaying different average content of *F*-ligands. Indeed these sub-populations are likely to be formed only if the introduction of *F*-ligands results in the formation of clusters in the monolayer. A somewhat intermediate behaviour is displayed by nanoparticles **NP-C8/F6**; indeed, the graph of Figure 3E share some features with that obtained for nanoparticles **NP-brC12/F6** and nanoparticles **NP-C16/F6**. This is peculiar since given the absence of length mismatch between the two thiols, the composition of the monolayer as a function of the initial molar fraction of the *F*-ligand should display a trend similar to that obtained for nanoparticles **NP-C12/F10**.

3 Conclusions

In this study we reported an analysis of the synthetic conditions for the preparation of MMNPs displaying fluorinated and hydrogenated ligands of different length and steric bulk. The nanoparticles were synthesised either by exploiting the direct synthesis or by place exchange on preformed hydrogenated NPs. In most of the cases, the composition of the monolayer of MMNPs comprising fluorinated and hydrogenated ligands was found to be a non-linear function of the initial composition of the reaction mixture. The amount of fluorinated component introduced in the monolayer depends on the structures of the fluorinated and hydrogenated thiolates. The observed behaviours, including the deviations from the linearity, are consistent with the tendency of the fluorinated and hydrogenated species to self-sort and with the role of the length mismatch in triggering the formation of domains by contributing to the overall thermodynamics of the monolayer assembly. The solubility properties of the nanoparticles are also consistent with the formation of fluorinated and hydrogenated domains in the monolayer of these systems. Taken together, the data presented here suggest that for nanoparticles **NP-C16/F6**, that display the larger difference in thiolates length among the systems explored, the formation of the mixed monolayer is dominated by the initial formation of small nucleation centres and the further growth of the domains is cooperative. In the case of nanoparticles **NP-C12/F6** and **NP-C12/F10**, the formation of small domains is likely to occur, and to be favoured, even at very small loading of the fluorinated component. For nanoparticles **NP-brC12/F6** the experimental evidences fully support the absence of any organization of the monolayer, in agreement with the observation of Stellacci and co-workers[42] on the effect exerted by branched thiolates on the organization of mixed monolayer nanoparticles. Further specific experimental and theoretical investigations are in progress to assess the morphology of the monolayer of these MMNPs. Overall, the study presented here represents the first systematic approach aimed at defining a useful guideline for the design of synthetic strategies for the preparation of MMNPs. This work also displays that for MMNPs, the analysis of the monolayer composition as a function of the molar fraction of the reacting thiols used in the synthesis, may provide information on the tendency of the thiolates to cluster on the surface of nanoparticles.

4 Experimental

Synthesis

Synthesis of MMNPs. The synthesis of the MMNPs **NP-C12/F6** and **NP-C12/F10** was performed by place exchange from **NP-C12** prepared according to a literature procedure.[47] The synthesis of **NP-C8/F6**, **NP-brC12/F6**, **NP-C16/F6**, was performed by the Brust-Schiffrin[53] method using a mixture of hydrogenated and fluorinated thiols. The general procedure for the syntheses are outlined below, synthetic details are reported in Table S1 for **NP-C12/F6**; Table S2 for **NP-C12/F10**; Table S3 for **NP-brC12/F6**; Table S5 for **NP-C8/F6** and Table S7 for **NP-C16/F6**. Characterization data are presented in Table S1 for **NP-C12/F6**; Table S2 for **NP-C12/F10**; Table S4 for **NP-brC12/F6**; Table S6 for **NP-C8/F6** and Table S8 for **NP-C16/F6**.

General procedure for Place exchange reaction

*Nanoparticles **NP-C12/F6** and **NP-C12/F10***. A solution of **NP-C12** dissolved in DCM at a concentration of 2 mg/ml was deoxygenated and used for the synthesis. To the nanoparticles, was added a solution of fluorinated thiols in deoxygenated DCM (the proper amount is reported in Table S1 for **NP-C12/F6** and Table S2 for **NP-C12/F10**). The reaction mixture was kept stirring at 40 °C in a pressure-tight screw-capped reaction vessel for three days. After this time the solution was concentrated to a small volume (about 5 mL) and the nanoparticles were precipitated by addition of methanol. The supernatant was discarded and the precipitated nanoparticles were taken-up in 1 mL of $CHCl_3$ and precipitated a second time by addition of methanol. The supernatant was discarded and the solid residue was dissolved in a small amount of $CHCl_3$ and transferred in a centrifuge tube. The solvent was removed by aid of a gentle argon stream and then the residue was washed with methanol (4 x 20 mL) and acetone (4 x 20 mL). To improve the purification process, the nanoparticles were dissolved in $CHCl_3$, the solvent was removed under an argon flux, and residue washed with methanol (4 x 20 mL) and acetone (4 x 20 mL). The purified nanoparticles were subjected to selective extractions first with $CHCl_3$ and afterwards with hexane. The insoluble material eventually present was tested for solubility in hexafluorobenzene. All of the fractions were

characterised by ^{1}H NMR, UV-VIS, TGA, TEM. Characterization data are reported in Table S1 for **NP-C12/F6** and Table S2 for **NP-C12/F10**.

General procedure for the direct synthesis of nanoparticles NP-brC12/F6, **NP-C8/F6 and NP-C16/F6.** A solution of tetraoctylammonium bromide, 2.5 equivalents, in DCM was added to an aqueous solution of $HAuCl_4 \cdot 3H_2O$ (1 equivalent), see Table S3 for **NP-brC12/F6**, Table S5 for **NP-C8/F6** and Table S7 for **NP-C16/F6**. The mixture was vigorously stirred observing fading of the aqueous phase while the organic phase turned orange. After the phase transfer was competed, a freshly prepared solution of the hydrogenated and fluorinated thiols in DCM was added to the reaction mixture. The concentration of the thiols solution and the volume used vary in the different syntheses. The total amount of thiols and their molar ratio are reported in Table S3 for **NP-brC12/F6**, Table S5 for **NP-C8/F6** and Table S7 for **NP-C16/F6**. The reaction mixture was left stirring at room temperature for 10 minutes and afterwards, a freshly prepared aqueous solution of $NaBH_4$ was added under vigorous stirring; the time required for adding the $NaBH_4$ solution is reported in Table S3 for **NP-brC12/F6**, Table S5 for **NP-C8/F6** and Table S7 for **NP-C16/F6**. The reaction mixture was left stirring for 18 hours at room temperature.

General procedures for work-up

*Nanoparticles **NP-brC12/F6** and **NP-C8/F6***. The organic and the aqueous layers were separated and the organic layer was washed with brine (1 x 20 mL) and the nanoparticles were precipitated by addition of methanol to the organic phase. The turbid suspension was transferred into two centrifuge tubes and centrifuged for 30 minutes at 4500 rpm at 15 °C. The supernatant was discarded and the solid residue was dissolved in 1 mL of $CHCl_3$; the nanoparticles were precipitated a second time by addition of methanol and recovered by centrifugation. After removal of the supernatant, the solid was washed with MeOH (3 x 15 mL) and acetone (3 x 15 mL). The purified nanoparticles were subjected to selective extractions with $CHCl_3$ and afterwards with hexane. The insoluble material eventually present was tested for solubility in hexafluorobenzene. All of the fractions were characterised by ^{1}H NMR, UV-VIS, TGA, TEM. Characterization data are reported in Table S4 for **NP-brC12/F6** and Table S6 for **NP-C8/F6**.

*Nanoparticles **NP-C16/F6.*** The organic and the aqueous layers were separated and the organic layer was washed with brine (1 x 20 mL). The nanoparticles were precipitated by addition of methanol. The turbid suspension was transferred into two centrifuge tubes and centrifuged for 3

minutes at 4500 rpm at 15 °C. The supernatant was discarded and the precipitate was washed with methanol. The crude nanoparticles preparation was recovered by centrifugation. The nanoparticles were dissolved with 1.0 mL of $CHCl_3$, the solvent was removed in an argon stream and the residue was washed with methanol (7 x 15 mL). The purified nanoparticles were subjected to selective extractions with $CHCl_3$ and afterwards with hexane. The insoluble material eventually present was tested for solubility in hexafluorobenzene. All of the fractions were characterised by ^{1}H NMR, UV-VIS, TGA, TEM. Characterization data are reported in Table S8.

Acknowledgements

This work was partly supported by the University of Trieste (FRA 2014, FRA 2015), FIRB 2011 Prot. RBAP11ETKA and MIUR: project MULTINANOITA. TEM images were recorded at the Microscopy Facility of the Department of Molecular Sciences and Nanosystems of the University Ca' Foscari of Venezia or at the Electron Microscopy Facility of the University of Trieste (with the assistance of Mr. Claudio Gamboz and Dr. Paolo Bertoncin).

References and notes

† **HF6** stands for 1*H*,1*H*,2*H*,2*H*-perfluorooctanethiol, with explicit reference to the sulfhydryl proton. The thiolate derived from 1*H*,1*H*,2*H*,2*H*-perfluorooctanethiol is reported as **F6**. All the thiols and thiolates in the text are named accordingly.

‡ **NP-C12/F10** stands for mixed monolayer nanoparticles displaying in the monolayer the thiolates derived from thiols **HC12** and **HF10**, all of the nanoparticle systems described in the text are named accordingly.

§ The number of alkanethiolate chains on the surface of gold nanoparticles as a function of the total number of gold atoms is fairly well described by the equation: $N° \; chains \cong 2.5 \; (NAu)^{-0.37}$. For nanoparticles with core size of 3.0 nm (976 gold atoms), the minimum theoretical Au/thiol ratio necessary to achieve passivation leaving no excess thiols is Au/thiols = 1/5. For these calculations, we used the data reported in reference 49.

[1] P. Pengo and L. Pasquato, *J. Fluorine Chem.*, 2015, **177**, 2–10.
[2] C. Gentilini, F. Evangelista, P. Rudolf, P. Franchi, M. Lucarini and L. Pasquato, *J. Am. Chem. Soc.* 2008, **130**, 15678−15682.
[3] T. Nishio, K. Niikura, Y. Matsuo and K. Ijiro, *Chem. Commun.* 2010, **46**, 8977–8979.
[4] K. Niikura, N. Iyo, Y. Matsuo, H. Mitomo and K. Ijiro, *ACS Appl. Mater. Interfaces* 2013, **5**, 3900−3907.
[5] K. Niikura, N. Iyo, T. Higuchi, T. Nishio, H. Jinnai, N. Fujitani and K. Ijiro, *J. Am. Chem. Soc.* 2012, **134**,7632−7635.

[6] M. Boccalon, S. Bidoggia, F. Romano, L. Gualandi, P. Franchi, M. Lucarini, P. Pengo and L. Pasquato, *J. Mater. Chem. B*, 2014, **3**, 432–439.
[7] M. Boccalon, P. Franchi, M. Lucarini, J. J. Delgado, F. Sousa, F. Stellacci, I. Zucca, A. Scotti, R. Spreafico, P. Pengo and L. Pasquato, *Chem. Commun.* 2013, **49**, 8794–8796.
[8] C. Gentilini, P. Franchi, E. Mileo, S. Polizzi, M. Lucarini and L. Pasquato, *Angew. Chem. Int. Ed.*, 2009, **48**, 3060–3064.
[9] P. Posocco, C. Gentilini, S. Bidoggia, A. Pace, P. Franchi, M. Lucarini, M. Fermeglia, S. Pricl and L. Pasquato, *ACS Nano*, 2012, **6**, 7243–7253.
[10] M. P. Krafft and J. G. Riess, *Chem. Rev.*, 2009, **109**, 1714–1792.
[11] J. D. Dunitz, *ChemBioChem*, 2004, **5**, 614–621.
[12] L. D. Zarzar, V. Sresht, E. M. Sletten, J. A. Kalow, D. Blankschtein and T. M. Swager, *Nature*, 2015, **518**, 520–524.
[13] N. C. Yoder, V. Kalsani, S. Schuy, R. Vogel, A. Janshoff, and K. Kumar, *J. Am. Chem. Soc.* 2007, **129**, 9037–9043.
[14] P. Long, and J. Hao, *Adv. Colloid Interface Sci.* 2012, **171-172**, 66–76.
[15] S. De Feyter and F. C. De Schryver, *J. Phys. Chem. B*, 2005, **109**, 4290–4302.
[16] M. Kadi, P. Hansson, M. Almgren and I. Furò, *Langmuir*, 2002, **18**, 9243–9249.
[17] V. Percec, M. R. Imam, M. Peterca and P. Leowanawat, *J. Am. Chem. Soc*. 2012, **134**, 4408–4420.
[18] V. Percec, M. Glodde, T. K. Bera, Y. Miura, I. Shiyanovskaya, K. D. Singer, V. S. K. Balagurusamy, P. A. Heiney, I. Schnell, A. Rapp, H.-W. Spiess, S. D. Hudsonk and H. Duank, *Nature*, 2002, **419**, 384–862.
[19] V. Percec, G. Johansson, G. Ungar and J. Zhou, *J. Am. Chem. Soc.*, 1996, **118**, 9855–9866.
[20] B. Bilgicüer, X. Xing and K. Kumar, *J. Am. Chem. Soc.* 2001, **123**, 11815–11816.
[21] B. C. Buer and E. N. G. Marsh, *Protein Sci.*, 2012, **21**, 453–462.
[22] A. Centrone, E. Penzo, M. Sharma, J. W. Myerson, A. M. Jackson, N. Marzari and F. Stellacci, *Proc. Natl. Acad. Sci. USA*, 2008, **105**, 9886–9891.
[23] A. Verma, O. Uzun, Y. H. Hu, Y. Hu, H. S. Han, N. Watson, S. L. Chen, D. J. Irvine and F. Stellacci, *Nat. Mater*. 2008, **7**, 588–595.
[24] A. Verma and Francesco Stellacci, *Small*, 2010, **6**, 12–21.
[25] R. C. Van Lehn, P. U. Atukorale, R. P. Carney, Y.-S. Yang, F. Stellacci, D. J. Irvine and A. Alexander-Katz, *Nano Lett.* 2013, **13**, 4060–4067.
[26] S. Jiang, Q. Chen, M. Tripathy, E. Luijten, K. S. Schweizer and S. Granick, *Adv. Mater.* 2010, **22**, 1060–1071.
[27] A. Ghosh, S. Basak, B. H. Wunsch, R. Kumar and F. Stellacci, *Angew. Chem. Int. Ed*., 2011, **50**, 7900 –7905.
[28] A. M. Jackson, J. W. Myerson and F. Stellacci, *Nat. Mat.* 2004, **3**, 330–336.
[29] A. M. Jackson, Y. Hu, P. J. Silva and F. Stellacci, *J. Am. Chem. Soc*. 2006, **128**, 11135–11149.
[30] A. Centrone, Y. Hu, A. M. Jackson, G. Zerbi, and F. Stellacci, *Small* 2007, **3**, 814–817.
[31] Q. K. Ong, J. Reguera, P. J. Silva, M. Moglianetti, K. Harkness, M. Longobardi, K.S. Mali, C. Renner, S. De Feyter and F. Stellacci, *ACS Nano*, 2013, **7**, 8529–8539.
[32] G. A. DeVries, M. Brunnbauer, Y. Hu, A. M. Jackson, B. Long, B. T. Neltner, O. Uzun, B. H. Wunsch and F. Stellacci, *Science* 2007, **315**, 358–361.
[33] H. Kim, R. P. Carney, J. Reguera, Q. K. Ong, X. Liu and F. Stellacci, *Adv. Mater*. 2012, **24**, 3857–3863.
[34] Y. Hu O. Uzun, C. Dubois and F. Stellacci, *J. Phys. Chem. C*, 2008, **112**, 6279–6284.
[35] O. Uzun, Y. Hu, A. Verma, S. Chen, A. Centrone and F. Stellacci, *Chem. Commun.*,2008, 196–198.
[36] C. Singh, P. K. Ghorai, M. A. Horsch, A. M. Jackson, R. G. Larson, F. Stellacci and S. C. Glotzer, *Phys. Rev. Lett.*, 2007, **99**, 226106-1–226106-4.
[37] I. C. Pons-Siepermann and S. C. Glotzer, *ACS Nano*, 2012, **6**, 3919-3924.

[38] C. Singh, A. M. Jackson, F. Stellacci and S. C. Glotzer, *J. Am. Chem. Soc.*, 2009, **131**, 16377–16379.
[39] A. Santos, C. Singh and S. C. Glotzer. *Phys. Rev. E*, 2010, **81**, 011113.
[40] R. P. Carney, G. A. DeVries, C. Dubois, H. Kim, J. Y. Kim, C. Singh, P. K. Ghorai, J. B. Tracy, R. L. Stiles, R. W. Murray, S. C. Glotzer and F. Stellacci, *J. Am. Chem. Soc*. 2008, **130**, 798−799.
[41] H. Singh, Y. Hu, B. P. Khanal, E. R. Zubarev, F. Stellacci and S. C. Glotzer, *Nanoscale* 2011, **3**, 3244–3250.
[42] X. Liu, M. Yu, H. Kim, M. Mameli and F. Stellacci, *Nat. Commun*. 2012, **3**,1182.
[43] F. Manea, C. Bindoli, S. Polizzi, L. Lay and P. Scrimin, *Langmuir*, 2008, **24**, 4120−4124.
[44] G. Guarino, F. Rastrelli, P. Scrimin and F. Mancin, *J. Am. Chem. Soc.,* 2012, **134**, 7200−7203.
[45] R. S. Ingram, M. J. Hostetler and R. W. Murray, *J. Am. Chem. Soc*. 1997, **119**, 9175−9178.
[46]R. Da Costa, M. Jurisch and J. Gladysz, *Inorg. Chim. Acta.*, 2008, **361**, 3205−3214.
[47] T. Shimizu, T. Teranishi, S. Hasegawa and M. Miyake, *J. Phys. Chem B*, 2003, **107**, 2719−2724.
[48] K. M. Harkness, A. Balinski, J. A. McLean and D. E. Cliffel, *Angew. Chem. Int. Ed.*, 2011, **50**, 10554 –10559.
[49] M. J. Hostetler, J. E. Wingate, C.-J. Zhong, J. E. Harris, R. W. Vachet, M. R. Clark, J. D. Londono, S. J. Green, J. J. Stokes, G. D. Wignall, G. L. Glish, M. D. Porter, N. D. Evans and R. W. Murray, *Langmuir*, 1998, **14**, 17−30.
[50] P. J. Krommenhoek, J. Wang, N. Hentz, A. C. Johnston-Peck, K. A. Kozek, G. Kalyuzhny and J. B. Tracy, *ACS Nano*, 2012, **6**, 4903–4911.
[51] V. H. Dalvia and P. J. Rosskya, *Proc. Natl. Acad. Sci. USA*, 2010, **107**, 13603−1307.
[52] Y. Wang, O. Zeiri, A. Neyman, F. Stellacci and I. A. Weinstock, *ACS Nano*, 2012, **6**, 629−640.
[53] M. Brust, M. Walker, D. Bethell, D. J. Schiffrin and R. Whyman, *J. Chem. Soc., Chem. Commun.*, 1994, 801−802.